Langmuir

Article

pubs.acs.org/Langmuir

Hyaluronic Acid Click Hydrogels Emulate the Extracellular Matrix

Shawn C. Owen,[†,‡,§] Stephanie A. Fisher,[†,‡,§] Roger Y. Tam,[†,‡,§] Chelsea M. Nimmo,[†,∥] and Molly S. Shoichet*[,†,‡,§,∥]

[†]The Donnelly Centre for Cellular and Biomolecular Research, [‡]Department of Chemical Engineering and Applied Chemistry, [§]Institute of Biomaterials and Biomedical Engineering, and [∥]Department of Chemistry, University of Toronto, 160 College Street, Room 514, Toronto, Ontario M5S 3E1, Canada

Supporting Information

ABSTRACT: Hydrogels are used to create 3D microenvironments with properties that direct cell function. The current study demonstrates the versatility of hyaluronic acid (HA)-based hydrogels with independent control over hydrogel properties such as mechanics, architecture, and the spatial distribution of biological factors. Hydrogels were prepared by reacting furan-modified HA with bis-maleimide-poly(ethylene glycol) in a Diels–Alder click reaction. Biomolecules were photopatterned into the hydrogel by two-photon laser processing, resulting in spatially defined growth factor gradients. The Young's modulus was controlled by either changing the hydrogel concentration or the furan substitution on the HA backbone, thereby decoupling the hydrogel concentration from mechanical properties. Porosity was controlled by cryogelation, and the pore size distribution, by the thaw temperature. The addition of galactose further influenced the porosity, pore size, and Young's modulus of the cryogels. These HA-based hydrogels offer a tunable platform with a diversity of properties for directing cell function, with applications in tissue engineering and regenerative medicine.

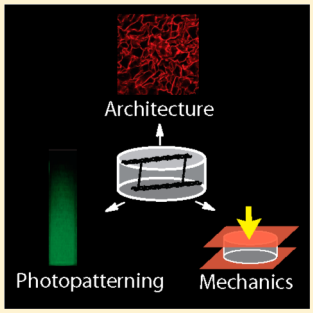

1. INTRODUCTION

Cells reside in a complex microenvironment of proteoglycans, proteins, and signaling molecules. This extracellular matrix (ECM) provides biophysical and biochemical instructions that guide cell growth, behavior, and fate (Figure 1A). Attempts to recreate the cell ECM in vitro using natural and synthetic scaffolds have identified specific properties that recapitulate in vivo attributes.[1] Many of the ECM properties are paramount in dictating cell growth and function, including the concentration and distribution of growth factors and binding ligands and architectural properties of scaffolds such as the porosity, mechanical stiffness, and density of tethering sites. ECM attributes guide proper stem cell differentiation, promote tissue regeneration, affect proliferation rates, enhance the migration potential, and even influence disease states such as cancer.[2−8]

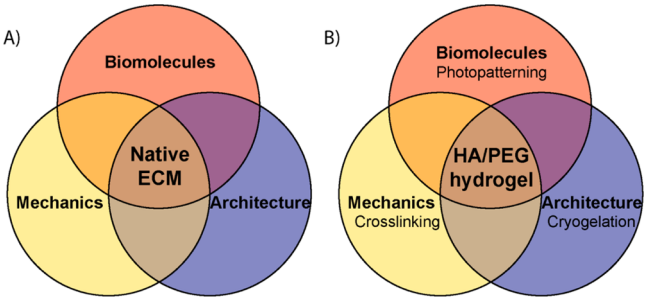

Figure 1. (A) Multiple properties in the extracellular matrix are essential to cell behavior. (B) Multiple aspects of HA-furan/PEG hydrogels can be simultaneously controlled to recapitulate native cell environments.

Hydrogels currently used in 3D cell culture and tissue engineering are created from chemically or physically cross-linked polymer systems.[9] Although these systems are robust and diverse, many lack the versatility to control the multiple properties important to cell function. The most promising platforms allow several biophysical and biochemical aspects of the ECM to be controlled and combined to provide unprecedented flexibility in recreating the desired native environment of a given cell. Indeed, those hydrogels that can be systematically modified to control the biochemical, architectural, and mechanical properties simultaneously will be most successful in recapitulating the diversity of native ECMs.

Hyaluronic acid (HA) is particularly compelling as a scaffold because it is a natural occurring nonsulfated glycosaminoglycan found ubiquitously in the ECM and is readily chemically modified to form hydrogels.[10,11] Building on our previous success in synthesizing HA-cross-linked hydrogels,[11] here we report HA-furan/bis-maleimide-poly(ethylene glycol) Diels–Alder click-cross-linked hybrid hydrogels that are tuned to mimic many of the properties of the ECM. Matrix biochemical cues are manipulated using two-photon patterning technology, matrix architecture is controlled by cryogenic gelation

Special Issue: Interfacial Nanoarchitectonics

Received: December 17, 2012
Revised: January 22, 2013
Published: January 24, 2013

   dx.doi.org/10.1021/la305000w | *Langmuir* 2013, 29, 7393−7400

conditions, and matrix mechanical properties are tuned by the matrix density and degree of cross-linking (Figure 1B).

2. EXPERIMENTAL SECTION

2.1. Materials. Dried sodium hyaluronate (HA) (2.34×10^5 amu), was purchased from Lifecore Biomedical (Chaska, MN, USA). Bis-(*N*-ethylmaleimide)-poly(ethylene glycol) (PEG-$(mal)_2$) (3.0×10^3 amu) was purchased from RAPP Polymere GmbH (Germany). 4-(4,6-Dimethoxy-1,3,5-triazin-2-yl)-4-methylmorpholinium chloride (DMTMM) and dimethyl sulfoxide (DMSO) were purchased from Sigma-Aldrich (St. Louis, MO, USA). Furfurylamine was purchased from Acros Organics (Belgium). 2-(*N*-Morpholino)-ethanesulfonic acid (MES) buffer and 2-[(2-hydroxy-1-bis[hydroxy methyl ethyl) aminoethanesulfonic acid (TES) buffer were purchased from Bioshop Canada Inc. (Burlington, ON, Canada). 5-Dulbecco's phosphate-buffered saline (PBS) was purchased from Multicell Technologies Inc. (Woonsocket, RI, USA). AlexaFluor 488-hydrazide and AlexaFluor 568-hydrazide were purchased from Invitrogen (Eugene, OR, USA). Dialysis membranes were purchased from Spectrum Laboratories Inc. (Rancho Dominguez, CA, USA). Recombinant human epidermal growth factor (EGF) was purchased from PeproTech Inc. (Rocky Hill, NJ, USA). Sulfosuccinimidyl[4-iodoacetyl]aminobenzoate (Sulfo-SIAB) and dialysis cassettes were purchased from Thermo-Fisher (Pittsburgh, PA, USA).

2.2. Synthesis and Characterization of HA-Furan and Coumarin-HA-Furan. Furan-modified HA derivatives (HA-furan) were synthesized as previously described.[11] Briefly, HA-furan derivatives were prepared by dissolving HA (0.40 g, 1.04 mmol carboxylates) in 40 mL of MES buffer (100 mM, pH 5.5). To prepare 40%-substituted HA-furan, DMTMM (0.25 g, 1.02 mmol, 1 equiv) was added to the mixture and stirred for 10 min. Furfurylamine (47.2 μL, 0.50 mmol, 0.5 equiv) was then added dropwise to the solution. To prepare 55%-substituted HA-furan, DMTMM (0.56 g, 2.04 mmol, 2 equiv) and furfurylamine (94.4 μL, 1.02 mmol, 1 equiv) were used. The reaction was stirred at room temperature for 24 h and then dialyzed against distilled water for 3 days (M_w cutoff 12−14 kDa). Water was removed by lyophilization to obtain HA-furan derivatives as a white powder. The degree of substitution (DS) was determined from ^{1}H NMR spectra by comparing the ratio of the areas under the proton peaks at 6.26, 6.46, and 7.65 ppm (furan protons) to the peak at 1.9 ppm (*N*-acetyl glucosamine protons of HA). ^{1}H NMR spectra were recorded in D_2O on a Varian Mercury-400 MHz NMR spectrometer (Palo Alto, CA, USA).

Derivatives of 6-bromo-7-hydroxycoumarin sulfide (coumarin) were prepared according to a published procedure[12] and conjugated to HA-furan carboxylates with DMTMM to form coumarin HA-furan derivatives (coumarin-HA-furan). HA-furan (0.526 g, 1.194 mmol carboxylates) was dissolved in 50 mL of MES buffer (100 mM, pH 5.5). Following complete dissolution, DMTMM (0.066 g, 0.23988 mmol, 0.2 equiv) in 300 μL of MES buffer (100 mM, pH 5.5) was added, and the reaction mixture was stirred for 30 min. Coumarin (0.0394 g, 0.1194 mmol, 0.1 equiv) in 100 μL of DMSO was then added dropwise, and the reaction was stirred in the dark at room temperature for 24 h (Supporting Information Figure 1). The reaction solution was then dialyzed in the dark against distilled water for 3 days (M_w cutoff 12−14 kDa) and lyophilized in the dark to obtain coumarin-HA-furan as a fluorescent, white spongy powder (λ_{abs} = 335 nm). The DS was determined from ^{1}H NMR.

2.3. General Preparation of HA-Furan/PEG Hydrogels. HA-furan hydrogels cross-linked with bis-maleimido-poly(ethylene glycol) (PEG-$(mal)_2$) via Diels−Alder chemistry were synthesized as previously described.[11] In a representative example (100 μL of hydrogel with an HA concentration of 1.0% w/v), HA-furan (1.00 mg, 1.0 equiv of furan) was dissolved in 73 μL of MES buffer, and PEG-$(mal)_2$ (1.37 mg, 1.0 equiv of maleimide) was dissolved in 23 μL of MES buffer (100 mM, pH 5.5). The two solutions were mixed thoroughly and allowed to react overnight to give HA-furan or coumarin-HA-furan hydrogels cross-linked with PEG (Figure 2).

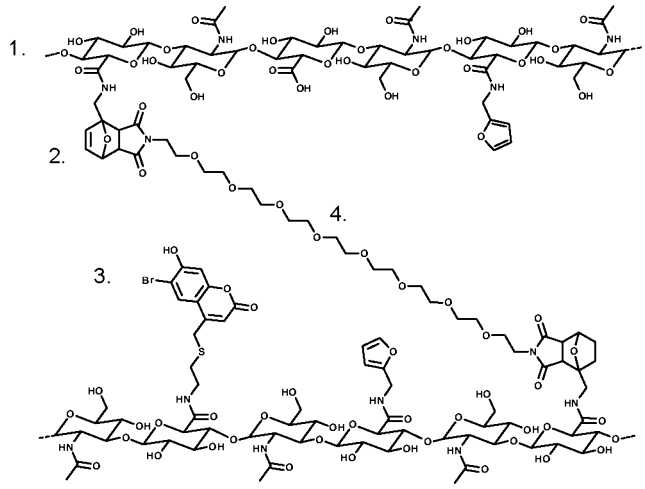

1. Hyaluronic acid backbone modified with furan
2. Diels-Alder "click" conjugate between furan and maleimide
3. UV-sensitive coumarin-protected thiol
4. PEG crosslinker

Figure 2. HA-furan backbone cross-linked with PEG via Diels−Alder click chemistry to afford HA-furan/PEG hydrogels. A photolabile coumarin moiety can also be incorporated for 3D patterning of iodoacetamide-functionalized biomolecules.

2.4. Synthesis and Characterization of IA-EGF-488. EGF was modified with an iodoacetamide functionality and a fluorescent dye for patterning and visualization purposes, respectively (Supporting Information Figure 2). EGF (2.0 mg, 0.32 μmol) was dissolved in TES buffer (50 mM, pH 8.6), to which sulfo-SIAB (4.0 mg, 8.1 μmol, 25 equiv) was added every 2 h at room temperature until a 100 molar total excess of sulfo-SIAB was reached. Iodoacetylated-EGF (IA-EGF) was purified by dialysis for 48 h (M_w cutoff 2 kDa) against TES (50 mM, pH 8.0) at 4 °C with frequent buffer changes. The degree of iodoacetylation was determined using MALDI-TOF (MDS Sciex API QSTAR XL Pulsar MALDI QTOF, Applied Biosystems, Foster City, CA).

IA-EGF (1.0 mg, 0.16 μmol) in MES (50 mM, pH 5.5) was combined with DMTMM (4.4 mg, 160 μmol, 100 equiv) and AlexaFluor 488-hydrazide (2.0 mg, 35 μmol, 20 equiv). The reaction mixture was agitated at room temperature for 24 h. The fluorescently labeled protein (IA-EGF-488) was purified by dialysis for 48 h (M_w cutoff 2 kDa) against PBS (pH 7.4) with frequent buffer changes. The substitution level of AlexaFluor 488 per mole of IA-EGF was calculated according to the manufacturer's instructions (Invitrogen, Eugene, OR). An extinction coefficient of 17 780 M^{-1} cm^{-1} at λ = 280 nm was used for IA-EGF. See the Supporting Information for detailed results.

2.5. Photopatterning of IA-EGF-488 within HA-Furan/PEG Hydrogels. Preformed gels of 100 μL of coumarin-HA-furan/PEG samples were incubated in 100 μL of PBS (100 mM, pH 8.5) at room temperature for 8 h following gelation. A 90 μL solution of IA-EGF-488 (0.17 mg/mL) was added on top of the gels and left for 16 h at room temperature. A region of interest (ROI) (100 μm × 100 μm) was drawn into the hydrogel, 100 μm relative to the glass bottom. The microscope stage position and laser parameters were controlled using control scripts written in-house using the Leica/Visual Basic software interface. A scanned grid of square ROIs, increasing the number of scans for each subsequent square by 5, resulted in 10 squares being scanned from 5 to 50 times. The coumarin-HA-furan/PEG hydrogels were then submerged in PBS buffer (100 mM, pH 7.4) for 48 h to remove excess protein.

To convert the fluorescence intensity into protein concentration, a calibration curve was constructed with AlexaFluor 488. Hydrogel samples with Alexa 488 concentrations of 0, 20, 100, 500, 1000, 2500, and 5000 nM were imaged 100 μm into the hydrogel, relative to the

glass bottom. The calibration curve, along with the known number of fluorophores per protein, was used to calculate the protein concentration.

2.6. Confocal Settings for Photopatterning and Fluorescence Imaging. All patterns were created using a Leica TCS-SP2 confocal microscope (Leica Microsystems, Wetzlar, Germany) equipped with a multiphoton Mai Tai broadband Ti-sapphire laser (Spectra-Physics) using a 20× objective (NA = 0.4) and an electronic stage. The multiphoton laser was set to 740 nm with an offset of 75% and a gain of 43% for patterning.

Images were collected by confocal microscopy on an Olympus FV1000 at 20× magnification using the following excitation and emission wavelengths: for Alexa-488, excitation at 485 nm, emission at 520 nm; for Alexa-546, excitation at 560 nm, emission at 580 nm. ImageJ was used for fluorescence quantification.

2.7. Preparation of HA-Furan/PEG Cryogels. HA-furan (40% substitution, 10.00 mg, 1.0 equiv of furan) was dissolved in 0.5 mL of MES buffer (10 mM, pH 5.5). For sugar-modified formulations, D-galactose was added (39.6 mg, 220 μmol) to the HA-furan and mixed. The viscous liquid was cooled to 4 °C and degassed for 1 min to remove any air bubbles. In another vial, PEG-$(mal)_2$ cross-linker (13.65 mg, 1.0 equiv of maleimide) was dissolved in 0.5 mL of MES buffer (10 mM, pH 5.5), cooled to 4 °C, and carefully mixed with the solution containing HA-furan. The mixture was then flash frozen in liquid nitrogen and maintained at either −6 or −15 °C for 8 h. The solutions were then warmed to room temperature for 1 h, followed by another identical freeze/thaw cycle. The reactions were quenched by adding 10 mg/mL *N*-ethylhydroxy maleimide (0.2 mL) and incubated overnight at room temperature.

2.8. Pore Size Characterization. Unreacted carboxylates of the HA-furan polysaccharide backbone were conjugated to AlexaFluor 568-hydrazide using DMTMM chemistry to enable the visualization of the pore size and pore wall thickness. HA-cryogels were diluted with MES buffer (100 mM, pH 5.5), followed by the addition of DMTMM (4 mg, 15 μmol) and AlexaFluor 568-hydrazide (1 mg, 1.75 μmol) and mixed overnight at room temperature in the dark. The labeled gels were washed extensively with MES buffer, followed by distilled water. Three Z-stack sections of each gel were then imaged on an Olympus confocal microscope at 20× magnification. Three images from each Z stack were analyzed for pore size using ImageJ software.

2.9. Mechanical Compression Testing. The Young's moduli were determined for HA-furan/PEG hydrogels and cryogels that had been preswollen in PBS for a day and formed into cylindrical samples with a diameter of 5 mm. Samples were placed between two impermeable flat platens connected to a DAQ-Nano17 force transducer (ATI Industrial Automation) on a Mach-1 micromechanical system (Biomomentum). Samples were subjected to an initial tare force of 0.01 N to even out surface defects, and the platen-to-platen separation was taken as the initial sample height. Uniaxial, unconfined compression was performed at 37 °C at a deformation rate of 10 μm/s until an applied strain of 20% was reached. The Young's modulus was taken as the slope of the resultant stress versus strain chart for each sample.

2.10. Statistical Analysis. All statistical analyses were performed using GraphPad Prism version 5.00 for Windows (GraphPad Software, San Diego, CA, USA, www.graphpad.com). Differences among groups of three or more treatments were assessed by one-way ANOVA with either Bonferroni or Newton-Keuls post hoc corrections to identify statistical differences. Differences among two treatments were assessed using unpaired *t* tests. An α level of 0.05 was set as the criterion for statistical significance. Graphs are annotated with *p* values represented as * ≤ 0.05, ** ≤ 0.01, or *** ≤ 0.001. All data are presented as mean ± standard deviation.

3. RESULTS AND DISCUSSION

3.1. Synthesis of HA-Furan and Coumarin-HA-Furan with Control over the Degree of Substitution. HA-furan was synthesized as previously reported to give a furan substitution level of 40 or 55% by altering the ratio of HA to furfurylamine and DMTMM. HA-furan was further modified with coumarin derivatives to give photosensitive coumarin-HA-furan conjugates used for patterning experiments (Figure 3). The degree of substitution of coumarin was controlled to between 1 and 4% by altering the reaction conditions.

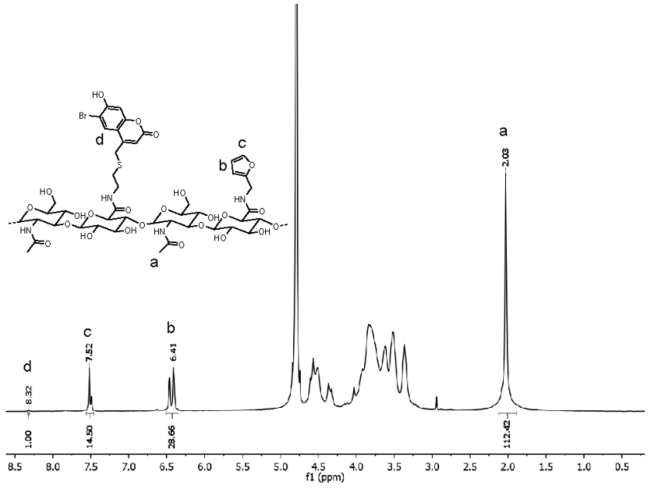

Figure 3. Typical ^{1}H NMR for coumarin-HA-furan with 40% furan and 1% coumarin substitution. The degree of substitution is determined from the integration of respective peaks: HA (peak a), furan (peaks b and c), and coumarin (peak d).

PEG-$(mal)_2$ is compelling as a cross-linker because it provides the hydrogel with a blank palette in which to introduce biologically active molecules. The potential to tune this HA hydrogel with any bis-maleimide cross-linker gives these gels greater versatility than what can be achieved using collagen or similar gels with coupled concentration and mechanics.

3.2. Patterning of IA-EGF-488 within Coumarin-HA-Furan/PEG Hydrogels. To verify our ability to immobilize iodoacetamide-functionalized EGF labeled with AlexaFluor 488 (IA-EGF-488) in spatially defined patterns, IA-EGF-488 was added to photolabile coumarin-HA-furan/PEG hydrogels (1% DS for coumarin). Two-photon excitation at 740 nm in 3D space generated a pattern of free thiols, which in turn reacted with IA-EGF-488 through a bimolecular nucleophilic substitution reaction, ultimately to yield HA-EGF-488 (Supporting Information Figure 3).

We first patterned a series of squares (100 × 100 μm^2) 100 μm below the surface of the hydrogel. By increasing the irradiation exposure of the HA hydrogels to the multiphoton Ti/sapphire confocal laser, the concentration of exposed thiols increased, resulting in greater amounts of IA-EGF-488 immobilized within the hydrogels (Figure 4A).

A volume that was scanned five times resulted in an immobilized protein concentration of 52 ± 2 nM. Increasing the number of scans to 50 increased this immobilized protein concentration to 508 ± 2 nM. A linear relationship between the irradiation exposure and the amount of immobilized protein is evident (Figure 4B) and consistent with previous 3D patterning reports in other hydrogels, thereby demonstrating the applicability of this technique to diverse transparent hydrogels.[13−15] Additional control of protein immobilization can also be achieved by either altering the degree of substitution of the coumarin functionality on the HA backbone or varying the laser intensity.

dx.doi.org/10.1021/la305000w | *Langmuir* 2013, 29, 7393−7400

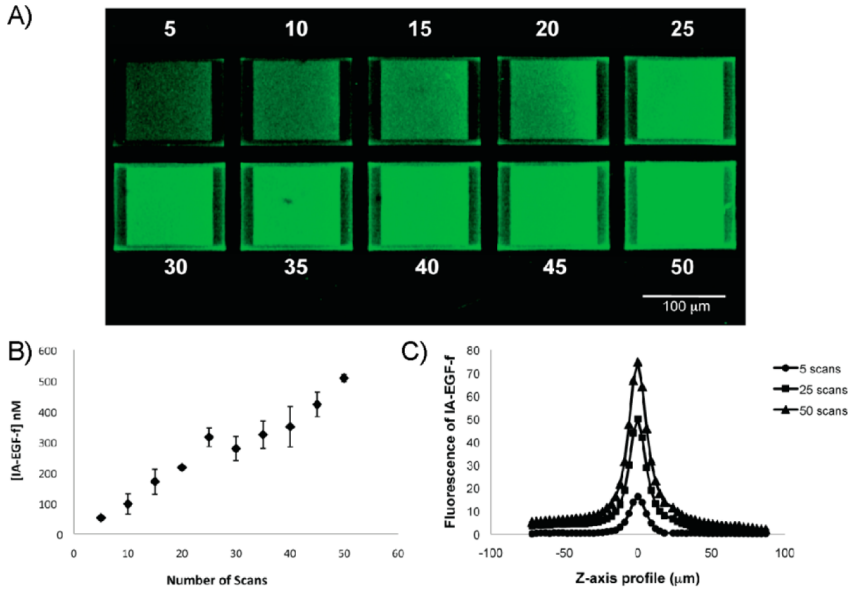

Figure 4. Controlled 3D immobilization of EGF within HA-furan/PEG hydrogels. (A) Ten different squares (100 × 100 μm^2) were patterned 100 μm into the hydrogel, with each region being exposed to an increasing number of scans ranging from 5 to 50. (B) The concentration of IA-EGF-488 immobilized per number of scans was quantified by measuring the fluorescence from each square in comparison to a standard curve of HA hydrogels with known concentrations of Alexa 488 (mean ± S.D., n = 3). (C) The z-axis profile of the fluorescence of IA-EGF-488 for boxes with 5, 25, and 50 scans was plotted, with the maximum intensity centered at 0 μm.

A plot of the fluorescence profile of IA-EGF-488 against position within the z axis confirmed that the patterned volumes of protein were in fact distributed in three dimensions (Figure 4C). For a graphical representation, the maximum fluorescence was set at 0 μm, and the distribution of immobilized IA-EGF-488 within the z plane of the coumarin-HA-furan/PEG hydrogel was visualized. The fluorescence intensity profile along the z axis for all squares spans approximately 30 μm for 5 scans to 100 μm for 50 scans. As expected, increasing the number of scans results in a broader profile, given that the excitation volume of the two-photon laser is increased along the z axis with irradiation exposure. All patterns maintained their shape, size, and fluorescence after 2 weeks in an aqueous buffer (Supporting Information Figure 4), demonstrating that the thioether bonds formed during the patterning process are stable.

To date, the 3D patterning of biomolecules has been performed only in hydrogels composed of non-native or synthetic materials such as agarose[12−15] or PEG.[16] This work presents, for the first time, the 3D immobilization of proteins within a hybrid hydrogel system consisting of the natural ECM proteoglycan HA and the synthetic polymer PEG.

3.3. Photopatterning of Gradient Channels of IA-EGF-488. Three-dimensional patterning of proteins within tissue engineering scaffolds represents a sophisticated technique for harnessing spatial control over cellular activities such as cell migration, differentiation, and proliferation.[17−19] Agarose hydrogels with linear concentration gradients of immobilized proteins have been shown.[13,20] In this study, we demonstrated that the 3D patterning of protein gradients can be extended to our HA-furan/PEG hydrogel. To prepare concentration gradients of functionalized proteins, coumarin-HA-furan/PEG hydrogels containing IA-EGF-488 were irradiated over a defined region of interest within the hydrogels. By taking advantage of the correlation between increased EGF immobilization with increased two-photon irradiation shown in Figure 4, we increased the number of scans with increased depth in the hydrogel. This technique created concentration gradients of EGF from 25 to 250 nM over 150 μm (Figure 5).

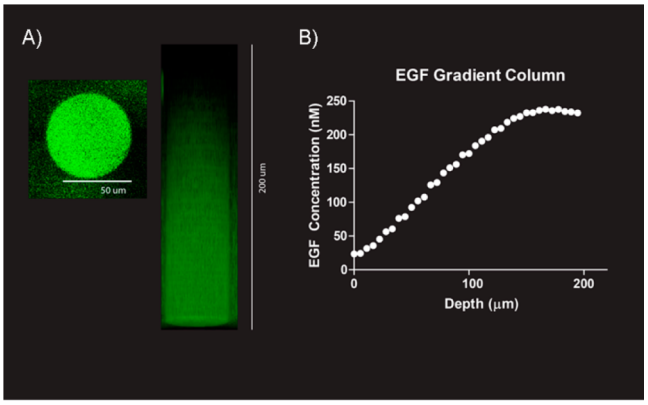

Figure 5. Three-dimensional patterning of EGF within a coumarin-HA-furan/PEG hydrogel. (A) Creation of a linearly immobilized gradient of EGF. From the top of the hydrogel, the number of scans by the multiphoton laser is increased as it penetrates the sample, corresponding to an increase in fluorescence intensity and hence an increase in protein immobilization. (B) The concentration of immobilized protein in the gradient was quantified by the fluorescence intensity, showing a change in concentration from 25 nM at the top of the hydrogel to 250 nM at a depth of 150 μm in the hydrogel.

The ability to pattern biomolecules in defined volumes provides great control over the distribution of biomolecules within biomimetic matrices. Chemical gradients of growth factors in the ECM are significantly important in guiding cell migration, development, and growth.[21] One specific example is found in vasculogenesis where gradients of vascular endothelial growth factor (VEGF) guide the budding and maturation of endothelial cells in blood vessel formation.[13] Gradients of EGF have been shown to guide the migration of mesenchymal stem cells[22] and significantly influence downstream transduction

dx.doi.org/10.1021/la305000w | Langmuir 2013, 29, 7393−7400

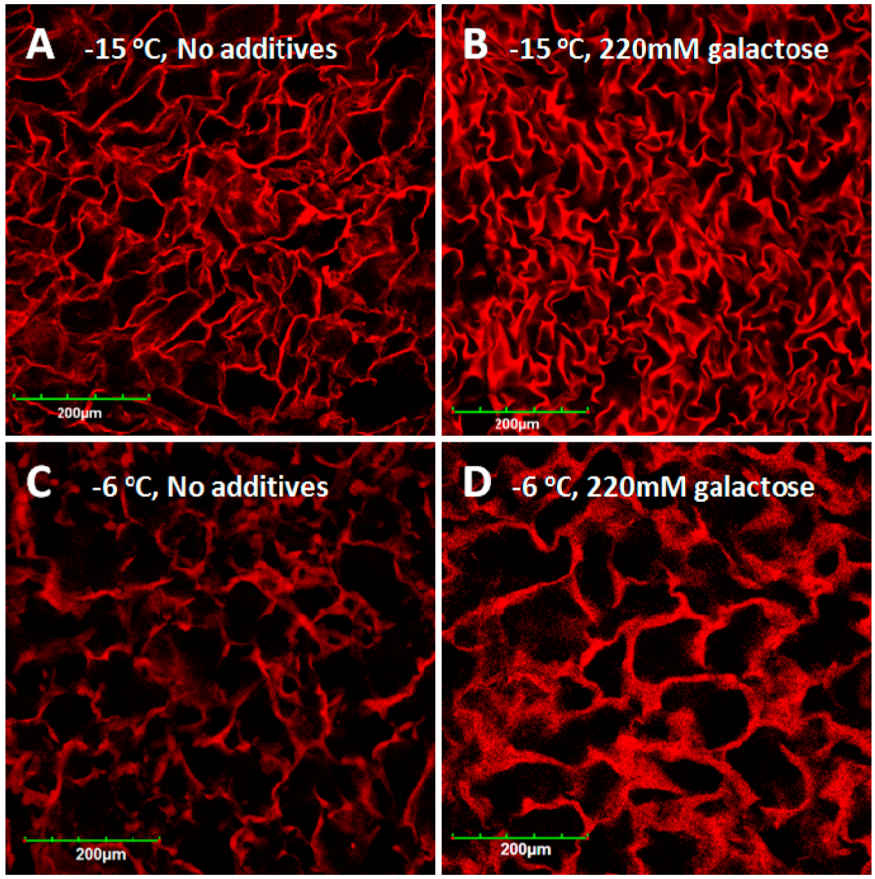

Figure 6. Effect of thawing temperature and presence of galactose on HA-furan/PEG cryogels fluorescently labeled with AlexaFluor 546. Confocal images of HA-furan/PEG cryogels that were formed at (A) a −15 °C thaw temperature, (B) a −15 °C thaw temperature in the presence of 220 mM galactose, (C) a −6 °C thaw temperature, and (D) a −6 °C thaw temperature in 220 mM galactose.

events through extracellular signal-related kinase (ERK) activation.[23] Chemical gradients of EGF are also important in the progression of many diseases, including cancer, where they influence the metastatic potential and cell migration.[24,25]

3.4. Macroporous HA-Furan/PEG Cryogels. The hydrogel pore size has been shown to influence cell behavior such as motility, attachment, and growth.[26,27] Therefore, we sought to develop a method to control the pore sizes formed in the HA-furan/PEG gels. Macroporous HA-furan/PEG gels were formed using a cryogelation technique previously described for poly(vinyl alcohol) hydrogels.[28,29] HA-furan and PEG-$(mal)_2$ were mixed together and immediately flash frozen to form ice crystals, concentrating solutes into the intergranular space between ice crystals. The presence of ice crystals acts to form the pores, resulting in macroporous hydrogels. Consistent with the properties of macroporous cryogels,[29] the HA-furan/PEG cryogels were spongy hydrogels with interconnected pore networks.

The temperature and presence of carbohydrates have been shown to affect the size of ice crystals during recrystallization.[30−32] Thus, the cryogelation of HA-furan/PEG was performed using various thawing temperatures (−15 or −6 °C). This provided a diverse set of cryogels with different pore sizes. The porosity of our hydrogel was controlled by producing gels under a range of conditions. Pore sizes were measured from confocal microscopy images of fluorescently labeled HA-furan/PEG cryogels (Figure 6A−D). This technique enables the quantification of pore sizes in the gel's hydrated state using ImageJ software.

The initial freezing of aqueous solutions resulted in the formation of small ice crystals, which recrystallize to form larger ice crystals as the temperature is gradually increased from −196 to −15 or −6 °C. Consistent with the theory that the size of the ice crystals corresponds to the thawing temperature,[31] we determined that an increase in the thawing temperature from −15 °C to −6 °C results in a significant difference in the pore size distribution in the cryogels. There is a decrease in the ratio of pore sizes of less than 100 μm relative to those above 100 μm (33 ± 11 and 16 ± 4 μm, $p < 0.05$) as the thawing temperature increased (Figure 7A).

Next, we investigated the effects of carbohydrate content on pore size. Interestingly, cryogelation formulations containing 220 mM galactose did not change the ratio of pores less than 100 μm to that greater than 100 μm (Figure 7A); however, the inclusion of 220 mM galactose resulted in significant differences ($p < 0.05$) in the number of pores smaller than 50 μm compared to those of formulations at the same respective temperatures (Figure 7B). At −15 °C, the presence of galactose increased the number of pores below 50 μm (from 239 ± 47 pores to 337 ± 68 pores), consistent with previous reports that galactose inhibits ice recrystallization.[32] Unexpectedly, at −6 °C, the presence of 220 mM galactose significantly decreased the number of smaller pores (from 203 ± 52 to 93 ± 16 pores). We hypothesize that the high carbohydrate concentration caused the colligative depression of the freezing/melting

dx.doi.org/10.1021/la305000w | *Langmuir* 2013, 29, 7393−7400

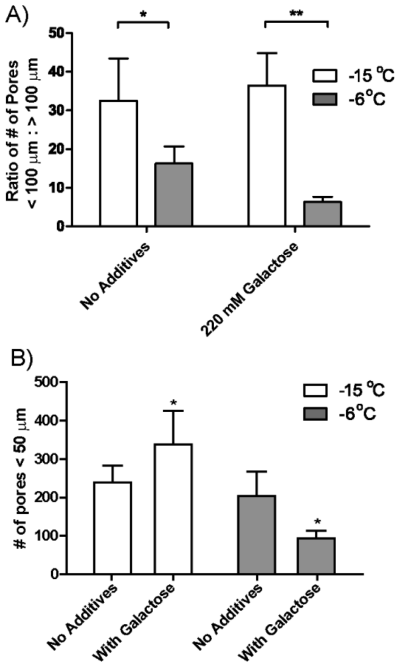

Figure 7. Effect of thawing temperature and presence of galactose on HA-furan/PEG cryogels. (A) Ratio of the number of pores <100 μm relative to the number of pores >100 μm. An increasing thawing temperature significantly decreases the ratio of small pores to large pores. (B) Number of pores <50 μm. In the presence of galactose, the total number of small pores in the hydrogel changes. (Values plotted are mean ± standard deviation, $n \geq 4$ samples, * $p < 0.05$, and ** $p < 0.01$.)

point of the reaction mixture, which consequently resulted in faster ice recrystallization and hence larger ice crystal sizes compared to those for cryogels prepared in the absence of carbohydrates.

The ability to tune the pore size is an important consideration for its use in biomedical applications,[33,34] and control of the pore size within the HA-furan/PEG hydrogels is advantageous because the gels can be tuned to match the optimal pore size required for a given application. For example, osteogenesis is achieved in scaffolds with pores >300 μm, and scaffolds with pores of 1−10 μm encourage fibroblast infiltration.[35,36]

3.5. Unconfined Compression Testing. An increase in hydrogel concentration produced significantly stiffer gels as shown by the increase in the Young's modulus (Figure 8A). The hydrogel's mechanical properties affect cell signaling.[2] For example, stiff matrices increase focal adhesions and integrin expression for many cell types,[37] which enhance signaling and alter cell behavior.[38] To control hydrogel mechanics, the hydrogel concentration is usually varied. However, increasing the hydrogel concentration also increases the number of matrix binding sites, which confounds the influence of matrix mechanics on cell behavior. To decouple the effects of matrix binding sites from mechanics, the furan substitution on the HA backbone was altered. With increasing furan substitution on HA, bis-maleimide cross-linkers of PEG have a greater chance of forming cross-links. The effect of furan substitution on hydrogel mechanics was demonstrated using 2% HA-furan/PEG hydrogels formed with either 40 or 55% furan-substituted HA, with both hydrogels containing the same initial concentration of PEG-$(mal)_2$ cross-linker. The higher furan

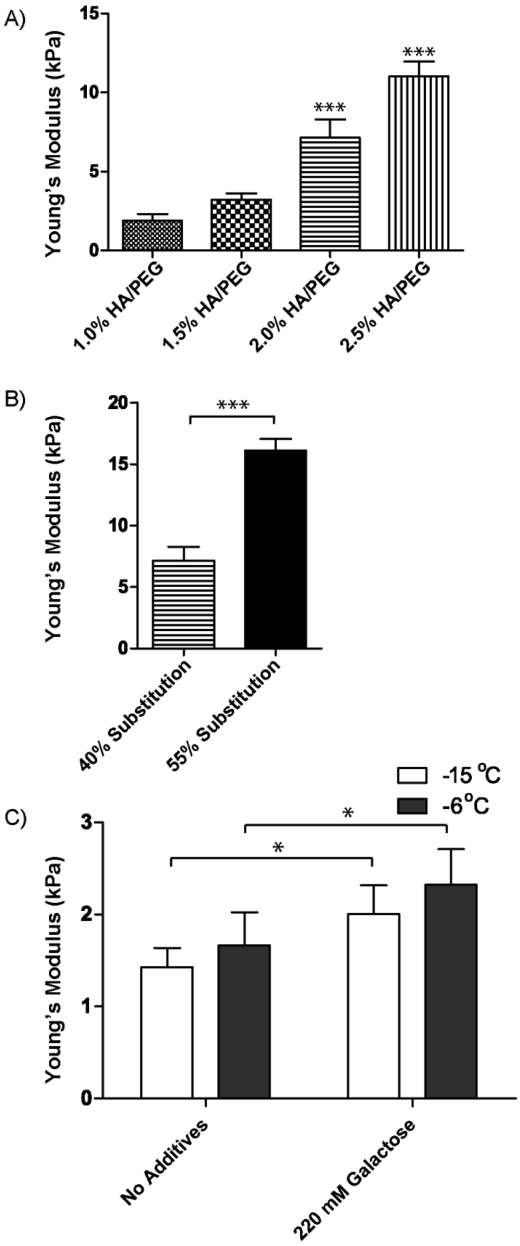

Figure 8. (A) Young's moduli of HA-furan/PEG hydrogels formed with 40% furan-substituted HA and a 1:1 ratio of furan/maleimide: and 1.0, 1.5, 2.0, and 2.5 HA-furan/PEG, $n \geq 5$, *** $p < 0.001$. (B) Young's moduli of 2% HA-furan/PEG hydrogels formed with 40 and 55% furan-substituted HA. The 40% HA-furan/PEG hydrogel had a 1:1 molar ratio of furan/maleimide. The 55% HA-furan/PEG hydrogels contained the same amounts of HA-furan and PEG-mal_2 as the 40% furan-substituted HA samples ($n = 6$, *** $p < 0.001$). (C) Young's moduli of HA-furan/PEG cryogels prepared at −15 or −6 °C thawing temperatures, with and without 220 mM galactose. The thawing temperature had no significant impact on the bulk mechanical properties of the cryogels, but the presence of galactose significantly increased the modulus in all preparations (*$p < 0.05$, $n = 4$).

substitution resulted in significantly stiffer hydrogels: from 7.14 ± 1.16 kPa for 40% substitution to 16.12 ± 0.94 kPa for 55% substitution. The difference was attributed to increased cross-linking between furan and maleimide (Figure 8B).

Comparatively, the Young's moduli of these cryogels are not significantly different than those of noncryogel HA-furan/PEG hydrogels. Interestingly, the stiffness of the HA-furan/PEG

dx.doi.org/10.1021/la305000w | Langmuir 2013, 29, 7393−7400

cryogels significantly increased in the presence of 220 mM galactose (Figure 5C, $p < 0.05$) but was not affected by the change in thawing temperature from −15 to −6 °C (Figure 8C). Gel stiffness is an intrinsic property that correlates with cross-linking reactions of the polysaccharide HA-furan backbone. The increase in the Young's modulus in galactose formulations may be due to an apparent increase in the concentration of unfrozen PEG molecules during the thawing process,[39] which in turn results in a greater number of reactive PEG-maleimide functional groups that react with the HA-furan backbone, thereby increasing the degree of cross-linking. When the thawing temperature and galactose concentration are altered, the micro- and macroscopic properties of the HA-furan/PEG hydrogel can be controlled.

Recently, collagen gels have been developed with independently tunable mechanics and collagen concentration.[40] Although an increased collagen concentration increased the proliferation of breast cancer cell line MDA-MB-231, the gel architecture had no effect.[40] In a separate study that decoupled gel stiffness from concentration, endothelial cells showed increased spreading, length, and number of angiogenic sprouts on stiffer collagen gels.[41] In the current study, the hydrogel mechanical properties can be varied by altering the degree of furan substitution and carbohydrate additives during cryogelation.

4. CONCLUSIONS

The current study demonstrates the versatility of hyaluronic acid (HA)-based hydrogels with independent control over biomolecule distribution, architecture topography, and mechanical properties. Simultaneous control over porosity and mechanical properties is instrumental in providing cells with a diverse set of ECM architectures. Importantly, we have also shown the ability to decouple the ECM density and mechanical properties by controlling the degree of furan substitution on the HA backbone. This represents an essential step forward in the ability to modulate single parameters of the ECM ultimately to elucidate their impact on cell function. Moreover, by introducing epidermal growth factor gradients, we demonstrate the breadth and versatility of the multiphoton laser patterning to HA-based hydrogels. The combined control over multiple facets of the biomimetic ECM provides a platform from which to answer biological questions in the broad fields of tissue engineering and regenerative medicine.

■ ASSOCIATED CONTENT

Supporting Information

Detailed synthesis schemes, mass spectra, and additional patterned images. This material is available free of charge via the Internet at http://pubs.acs.org.

■ AUTHOR INFORMATION

Corresponding Author

*E-mail: molly.shoichet@utoronto.ca. Phone: 416-978-1460. Fax: 416-978-4317.

Notes

The authors declare no competing financial interest.

■ ACKNOWLEDGMENTS

We are grateful for financial support from an NSERC Discovery Grant (M.S.S.), an NSERC Postgraduate Scholarship (S.A.F.), and an Alexander Graham Bell Canada Graduate Scholarship (C.M.N.). We thank members of the Shoichet research laboratory for thoughtful discussions, particularly Dr. Michael J. Cooke, Dr. Ryan G. Wylie, and Ms. Katarina Vulic.

■ REFERENCES

(1) Owen, S. C.; Shoichet, M. S. Design of three-dimensional biomimetic scaffolds. *J. Biomed. Mater. Res.* **2010**, *94A*, 1321−1331.
(2) Engler, A. J.; Sen, S.; Sweeney, H. L.; Discher, D. E. Matrix elasticity directs stem cell lineage specification. *Cell* **2006**, *126*, 677−689.
(3) Trappmann, B.; Gautrot, J. E.; Connelly, J. T.; Strange, D. G. T.; Li, Y.; Oyen, M. L.; Stuart, M. A. C.; Boehm, H.; Li, B. J.; Vogel, V.; Spatz, J. P.; Watt, F. M.; Huck, W. T. S. Extracellular-matrix tethering regulates stem-cell fate. *Nat. Mater.* **2012**, *11*, 642−649.
(4) Zeltinger, J.; Sherwood, J. K.; Graham, D. A.; Mueller, R.; Griffith, L. G. Effect of pore size and void fraction on cellular adhesion, proliferation, and matrix deposition. *Tissue Eng.* **2001**, *7*, 557−572.
(5) Berrier, A. L.; Yamada, K. M. Cell-matrix adhesion. *J. Cell. Physiol.* **2007**, *213*, 565−573.
(6) Bissell, M. J.; Radisky, D. Putting tumours in context. *Nat. Rev. Cancer* **2001**, *1*, 46−54.
(7) Ulrich, T. A.; Pardo, E. M. D.; Kumar, S. The mechanical rigidity of the extracellular matrix regulates the structure, motility, and proliferation of glioma cells. *Cancer Res.* **2009**, *69*, 4167−4174.
(8) Karp, J. M.; Dalton, P. D.; Shoichet, M. S. Scaffolds for tissue engineering. *MRS Bull.* **2003**, *28*, 301−306.
(9) Aizawa, Y.; Owen, S. C.; Shoichet, M. S. Polymers used to influence cell fate in 3D geometry: new trends. *Prog. Polym. Sci.* **2012**, *37*, 645−658.
(10) Burdick, J. A.; Prestwich, G. D. Hyaluronic acid hydrogels for biomedical applications. *Adv. Mater.* **2011**, *23*, H41−H56.
(11) Nimmo, C. M.; Owen, S. C.; Shoichet, M. S. Diels-Alder click cross-linked hyaluronic acid hydrogels for tissue engineering. *Biomacromolecules* **2011**, *12*, 824−830.
(12) Wosnick, J. H.; Shoichet, M. S. Three-dimensional chemical patterning of transparent hydrogels. *Chem. Mater.* **2008**, *20*, 55−60.
(13) Aizawa, Y.; Wylie, R.; Shoichet, M. Endothelial cell guidance in 3D patterned scaffolds. *Adv. Mater.* **2010**, *22*, 4831−4835.
(14) Wylie, R. G.; Ahsan, S.; Aizawa, Y.; Maxwell, K. L.; Morshead, C. M.; Shoichet, M. S. Spatially controlled simultaneous patterning of multiple growth factors in three-dimensional hydrogels. *Nat. Mater.* **2011**, *10*, 799−806.
(15) Wylie, R. G.; Shoichet, M. S. Three-dimensional spatial patterning of proteins in hydrogels. *Biomacromolecules* **2011**, *12*, 3789−3796.
(16) DeForest, C. A.; Anseth, K. S. Cytocompatible click-based hydrogels with dynamically tunable properties through orthogonal photoconjugation and photocleavage reactions. *Nat. Chem.* **2011**, *3*, 925−931.
(17) DeForest, C. A.; Polizzotti, B. D.; Anseth, K. S. Sequential click reactions for synthesizing and patterning three-dimensional cell microenvironments. *Nat. Mater.* **2009**, *8*, 659−664.
(18) Lee, S. H.; Moon, J. J.; West, J. L. Three-dimensional micropatterning of bioactive hydrogels via two-photon laser scanning photolithography for guided 3D cell migration. *Biomaterials* **2008**, *29*, 2962−2968.
(19) Luo, Y.; Shoichet, M. S. Light-activated immobilization of biomolecules to agarose hydrogels for controlled cellular response. *Biomacromolecules* **2004**, *5*, 2315−2323.
(20) Aizawa, Y.; Shoichet, M. S. The role of endothelial cells in the retinal stem and progenitor cell niche within a 3D engineered hydrogel matrix. *Biomaterials* **2012**, *33*, 5198−5205.
(21) Laurencin, C. T.; Nair, L. S.*Nanotechnology and Tissue Engineering: The Scaffold*; CRC Press: Boca Raton, FL, 2008.
(22) Miller, E. D.; Li, K.; Kanade, T.; Weiss, L. E.; Walker, L. M.; Campbell, P. G. Spatially directed guidance of stem cell population migration by immobilized patterns of growth factors. *Biomaterials* **2011**, *32*, 2775−2785.

(23) Kholodenko, B. N.; Hancock, J. F.; Kolch, W. Signalling ballet in space and time. *Nat. Rev. Mol. Cell Biol.* **2010**, *11*, 414−426.
(24) Nelson, C. M.; Bissell, M. J. Of extracellular matrix, scaffolds, and signaling: tissue architecture regulates development, homeostasis, and cancer. *Annu. Rev. Cell Dev. Biol.* **2006**, *22*, 287−309.
(25) Fischbach, C.; Chen, R.; Matsumoto, T.; Schmelzle, T.; Brugge, J. S.; Polverini, P. J.; Mooney, D. J. Engineering tumors with 3D scaffolds. *Nat. Methods* **2007**, *4*, 855−860.
(26) Harley, B. A. C.; Kim, H. D.; Zaman, M. H.; Yannas, I. V.; Lauffenburger, D. A.; Gibson, L. J. Microarchitecture of three-dimensional scaffolds influences cell migration behavior via junction interactions. *Biophys. J.* **2008**, *95*, 4013−4024.
(27) Ranucci, C. S.; Kumar, A.; Batra, S. P.; Moghe, P. V. Control of hepatocyte function on collagen foams: sizing matrix pores toward selective induction of 2-D and 3-D cellular morphogenesis. *Biomaterials* **2000**, *21*, 783−793.
(28) Hassan, C. M.; Peppas, N. A. Structure and Applications of Poly(vinyl alcohol) Hydrogels Produced by Conventional Cross-linking or by Freezing/Thawing Methods. In *Biopolymers, PVA Hydrogels, Anionic Polymerisation, Nanocomposites*; Chang, J. Y., Ed.; Springer: New York, 2000, Vol. *153*, pp 37−65
(29) Lozinsky, V. I.; Galaev, I. Y.; Plieva, F. M.; Savinal, I. N.; Jungvid, H.; Mattiasson, B. Polymeric cryogels as promising materials of biotechnological interest. *Trends Biotechnol.* **2003**, *21*, 445−451.
(30) Knight, C. A.; Hallett, J.; Devries, A. L. Solute effects on ice recrystallization - an assessment technique. *Cryobiology* **1988**, *25*, 55−60.
(31) Budke, C.; Heggemann, C.; Koch, M.; Sewald, N.; Koop, T. Ice recrystallization kinetics in the presence of synthetic antifreeze glycoprotein analogues using the framework of LSW theory. *J. Phys. Chem. B* **2009**, *113*, 2865−2873.
(32) Tam, R. Y.; Ferreira, S. S.; Czechura, P.; Chaytor, J. L.; Ben, R. N. Hydration index-a better parameter for explaining small molecule hydration in inhibition of ice recrystallization. *J. Am. Chem. Soc.* **2008**, *130*, 17494−17501.
(33) Slaughter, B. V.; Khurshid, S. S.; Fisher, O. Z.; Khademhosseini, A.; Peppas, N. A. Hydrogels in regenerative medicine. *Adv. Mater.* **2009**, *21*, 3307−3329.
(34) Mattiasson, B.; Kumar, A.; Galaev, I. *Macroporous Polymers: Production Properties and Biotechnological/Biomedical Applications*, CRC Press/Taylor & Francis: Boca Raton, FL, 2010.
(35) Karageorgiou, V.; Kaplan, D. Porosity of 3D biomaterial scaffolds and osteogenesis. *Biomaterials* **2005**, *26*, 5474−5491.
(36) Raeber, G. P.; Lutolf, M. P.; Hubbell, J. A. Molecularly engineered PEG hydrogels: a novel model system for proteolytically mediated cell migration. *Biophys. J.* **2005**, *89*, 1374−1388.
(37) Paszek, M. J.; Zahir, N.; Johnson, K. R.; Lakins, J. N.; Rozenberg, G. I.; Gefen, A.; Reinhart-King, C. A.; Margulies, S. S.; Dembo, M.; Boettiger, D.; Hammer, D. A.; Weaver, V. M. Tensional homeostasis and the malignant phenotype. *Cancer Cell* **2005**, *8*, 241−254.
(38) Mitra, S. K.; Schlaepfer, D. D. Integrin-regulated FAK-Src signaling in normal and cancer cells. *Curr. Opin. Cell Biol.* **2006**, *18*, 516−523.
(39) Izutsu, K.; Yoshioka, S.; Kojima, S.; Randolph, T. W.; Carpenter, J. F. Effects of sugars and polymers on crystallization of poly(ethylene glycol) in frozen solutions: phase separation between incompatible polymers. *Pharm. Res.* **1996**, *13*, 1393−1400.
(40) Carey, S. P.; Kraning-Rush, C. M.; Williams, R. M.; Reinhart-King, C. A. Biophysical control of invasive tumor cell behavior by extracellular matrix microarchitecture. *Biomaterials* **2012**, *33*, 4157−4165.
(41) Mason, B. N.; Starchenko, A.; Williams, R. M.; Bonassar, L. J.; Reinhart-King, C. A. Tuning three-dimensional collagen matrix stiffness independently of collagen concentration modulates endothelial cell behavior. *Acta Biomater.* **2013**, *9*, 4635−4644.